

***Final Draft***  
**of the original manuscript:**

Radjabian, M.; Koll, J.; Buhr, K.; Vainio, U.; Abetz, C.; Handge, U.A.;  
Abetz, V.:

**Tailoring the Morphology of Self-Assembled Block Copolymer  
Hollow Fiber Membranes**

In: *Polymer* (2014) Elsevier

DOI: [10.1016/j.polymer.2014.04.041](https://doi.org/10.1016/j.polymer.2014.04.041)

# Tailoring the Morphology of Self-Assembled Block Copolymer Hollow Fiber Membranes

Maryam Radjabian<sup>1</sup>, Joachim Koll<sup>1</sup>, Kristian Buhr<sup>1</sup>, Ulla Vainio<sup>2</sup>, Clarissa Abetz<sup>1</sup>, Ulrich A. Handge<sup>1</sup>, Volker Abetz<sup>1,3\*</sup>

<sup>1</sup> *Helmholtz-Zentrum Geesthacht, Institute of Polymer Research  
Max-Planck-Str.1, 21502 Geesthacht, Germany*

<sup>2</sup> *Helmholtz-Zentrum Geesthacht, Institute of Materials Research  
Max-Planck-Str.1, 21502 Geesthacht, Germany*

<sup>3</sup> *University of Hamburg, Institute of Physical Chemistry  
Grindelallee 117, 20146 Hamburg, Germany*

*\* Prof. Dr. Volker Abetz (Corresponding Author)*

*e-mail: [volker.abetz@hzg.de](mailto:volker.abetz@hzg.de)*

*Tel: +49 4152 872461*

*Fax: +49 4152 872499*

## **Abstract**

Isoporous asymmetric polystyrene-*block*-poly(4-vinylpyridine) (PS-*b*-P4VP) hollow fiber membranes were successfully made by a dry-jet wet spinning process. Well-defined nanometer-scale pores around 20-40 nm in diameter were tailored on the top surface of the fiber above a non-ordered macroporous layer by combining block copolymer self-assembly and non-solvent induced phase separation (SNIPS). Uniformity of the surface-assembled pores and fiber cross-section morphology was improved by adjusting the solution concentration, solvent composition as well as some important spinning parameters such as bore fluid flow rate, polymer solution flow rate and air gap distance between the spinneret and the precipitation bath. The formation of the well-organized self-assembled pores is a result of the interplay of fast relaxation of the shear-induced oriented block copolymer chains, the rapid evaporation of the solvent mixture on the outer surface and solvent extraction into the bore liquid on the lumen side, and gravity force during spinning. Structural features of the block copolymer solutions were investigated by small angle X-ray scattering (SAXS) and rheological properties of the solutions were examined as well. The scattering patterns of the optimal solutions for membrane formation indicate a disordered phase which is very close to the disorder-order transition. The nanostructured surface and cross-section morphology of the membranes were characterized by

scanning electronic microscopy (SEM). The water flux of the membranes was measured and gas permeation was examined to test the pressure stability of the hollow fibers.

Keywords: block copolymer, self-assembly, SNIPS, hollow fiber membrane, water flux

## **Introduction**

Among different geometrical shapes of membranes, the hollow fiber geometry has attracted much attention due to the high surface area per unit volume ratio, self-support and ease of module fabrication [1, 2]. During the last decades, many publications on mechanism formation and manufacturing developments of hollow fibers reveal a large significance and a high potential usage of these membranes for many applications [3-5]. Although production of hollow fiber membranes with both desirable morphology and separation performance is intriguing, the formation mechanism via phase inversion is more complex than for flat sheet membranes due to additional structure-controlling factors. However, a successful scheme of hollow fibers production via phase inversion is desirably leading to well-defined pore sizes, a narrow pore-size distribution, an ultrathin selective layer and an open-cell sponge-like substructure morphology in addition to proper mechanical properties and high separation performance [2].

Recently, a fascinating method for fabricating high-performance membranes with well-ordered pores combines the block copolymer self-assembly and non-solvent induced phase separation, abbreviated as SNIPS [6-8]. A unique feature of the SNIPS process is the formation of a continuously porous structure with periodic uniform pores on the top membrane surface by controlled solvent evaporation coupled with an immersion step in a suitable non-solvent. In a simple and fast process, a thin film of block copolymer in a specific solvent system is cast onto a substrate. Then the film solution is allowed to evaporate for a short time (usually tens of seconds) initiating microphase separation of the block copolymer at the surface of the film, before immersing into a precipitation bath [9, 10]. The first integral asymmetric membranes with highly uniform pore sizes created through the SNIPS procedure were successfully prepared from an asymmetrically composed amphiphilic polystyrene-*b*-poly(4-vinylpyridine) (PS-*b*-P4VP) diblock copolymer forming P4VP cylinders in a PS matrix. This diblock copolymer was dissolved in a mixture of tetrahydrofuran (THF, selective for PS) and dimethylformamide (DMF, selective for P4VP) [6]. During evaporation, after initiation of microphase separation, the higher volatility of THF leads to solidification of the PS matrix, while

DMF strongly swells the P4VP domains. During phase inversion the solvents are replaced by the precipitant (water) and this leads to an open porous structure, as in the top layer mainly DMF is present in the P4VP domains, while the PS matrix is already much more dense due to the evaporated THF [6,11]. Several works have been published on the formation of well-defined PS-*b*-P4VP membranes via the SNIPS process after the first publication [11-21] as these well-ordered nanostructured membranes have a great potential in many applications such as separation technologies, medical filtration, drug delivery and food industry.

The design of a SNIPS process to produce asymmetric block copolymer hollow fiber membranes with relatively good selectivity and permeability properties due to the assembled uniform nanometer-scale pores is a more challenging task. The fabrication of hollow fibers from block copolymers via the SNIPS procedure raises the number of control parameters to achieve a uniform pore separation layer on top of an asymmetric macroporous support. Shear stresses during extrusion, bore liquid non-solvent activity and gravitational force which becomes more prominent with increasing air gap are some of the important parameters in manufacturing hollow fibers in a dry/wet spinning process [1, 2 22-28]. In the SNIPS process of hollow fiber membranes, the volatile solvent is allowed to evaporate for a (short) time in the air gap. The suitable time frame to develop uniform pores can be tuned by adjusting the air gap as well as the polymer solution and bore fluid flow rate to compensate the destructive effect of high shear rate in the spinneret as well as avoiding the undesirable gravitational effect on the structure formation and pore shape. Furthermore, during the solvent evaporation in the air gap immediate solvent and non-solvent exchange between the spinning solution and the coagulating bore fluid increases the polymer concentration and induces precipitation from the lumen side.

In a previous study [29], the fabrication of asymmetric hollow fiber membranes of PS-*b*-P4VP block copolymers via the SNIPS method was reported for the first time. It is noteworthy that the combination of a dry/wet spinning procedure with block copolymer self-assembly makes the system more complicated. The non-linear behavior of shear viscosity as a function of shear rate indicates that the block copolymer solution undergoes structural changes leading to shear thinning. In this work on hollow fiber membranes, the rheological behavior of the PS-*b*-P4VP block copolymer solution in a mixture of DMF/THF was studied in order to investigate the influence of shear stress on the flow properties. To study the self-assembly and ordering in the suitable casting/spinning solutions, block copolymer micellization of PS-*b*-P4VP solution at different concentrations was also studied with

small-angle X-ray scattering (SAXS) measurements. We considerably focused on tailoring of the desired self-assembled pore morphology by changing the processing conditions in addition to the solution concentration and solvent composition.

## 2. Experimental section

### 2.1. Synthesis of PS-*b*-P4VP diblock copolymers

PS-*b*-P4VP diblock copolymer was synthesized by sequential anionic polymerization following the procedure described elsewhere [6]. The PS-*b*-P4VP compositions were determined by means of <sup>1</sup>H NMR spectroscopy. <sup>1</sup>H NMR spectra were recorded on a Bruker advance 300NMR spectrometer at 300 MHz with internal standard [tetramethylsilane (TMS)] using chloroform (CDCl<sub>3</sub>) as a solvent. The molecular weights of the precursors and polydispersities were measured by gel permeation chromatography (GPC) (Waters 2410 refractive-index detector) at 30 °C calibrated against polystyrene standards. The molecular characteristics of the block copolymers are listed in Table 1.

### 2.2. Production of hollow fiber membranes

All solutions were prepared by dissolving the block copolymers in a mixture of *N,N*-dimethyl formamide (DMF)/ tetrahydrofuran (THF) and stirring over a period of 48 h at ambient temperature to guarantee complete dissolution. The solutions were stored without disturbance for some hours to remove the effect of stirring and fine air bubbles entrapped in the solutions. In our experiments we used DURAN® GL 45 laboratory glass bottles with a particular tight sealing for long-term storage to avoid solvent evaporation.

Table 1. Characteristic properties of the PS-*b*-P4VP block copolymer and solutions

Block copolymer code <sup>a</sup>	PS [wt%]	P4VP [wt%]	M <sub>n</sub> [kg/mol]	PDI	Concentration [wt%]	DMF/THF [wt%]
PS <sub>82.7</sub> - <i>b</i> -P4VP <sub>17.3</sub> <sup>154</sup>	82.7	17.3	154	1.06	27	60/40
PS <sub>83.3</sub> - <i>b</i> -P4VP <sub>16.7</sub> <sup>168</sup>	83.3	16.7	168	1.06	24	50/50
PS <sub>81</sub> - <i>b</i> -P4VP <sub>19</sub> <sup>156</sup>	81	19	156	1.06	25	50/50

<sup>a</sup> Numbers in the subscript and superscript respectively indicate the weight percentage of each block and the total molecular weight in kg/mol

Hollow fiber membranes were fabricated from the block copolymer solutions using the well-known dry-jet wet spinning process via the SNIPS method. The process of hollow fiber spinning is schematically shown in Figure 1. A spinneret with an inner diameter equal to 0.628 mm, an annular

die gap equal to 0.337 mm for the polymer solution and a circular die with a diameter of 0.319 mm for the bore fluid was used. The bore fluid and polymer solution were extruded at controlled rates and passed through an air gap before immersing into the bath. Water was used as the bore fluid as well as the external coagulant in the immersion bath. The air gap distance between the spinneret and the coagulation bath allows evaporation of the volatile solvent from the nascent fibers and also solvent non-solvent exchange from the lumen side. In all cases, the spinning process was carried out at room temperature. The fabricated hollow fiber membranes were stored in fresh water for 24 h at room temperature to remove completely the residual solvents (which is mainly DMF) and were finally dried under vacuum over a period of 24 h at 60 °C. The spinning conditions are summarized in Table 2.

Table 2. Experimental parameters of hollow fiber spinning

Parameters	Range of variables
Polymer solution flow rate [ml/min]	0.6-5.0
Bore fluid flow rate [ml/min]	0.4-1.6
Air gap distance [cm]	1- 10
External/internal coagulant	Water
Dimension of spinneret [mm] ( $d_i$ : inner diameter/ $d_o$ : outer diameter)	1.303 /0.628
Spinning temperature [°C]	15-25

### 2.3. Rheological experiments

Rheological tests were performed using PS<sub>83.3</sub>-*b*-P4VP<sub>16.7</sub><sup>168</sup> solutions in a mixture of DMF/THF at a ratio of 60/40 wt%. Rheological experiments in oscillation and in rotation were carried out in order to elucidate the transient response of the solutions and to determine their viscous and elastic properties. A rotational rheometer (MCR 502, Anton Paar, Graz, Austria) was used for the experiments. A cone-plate geometry (plate diameter 25 mm, cone angle 2°) was used, and a nitrogen atmosphere was applied. The measurement temperature was 25 °C. The samples for rheological tests were prepared by stirring the block copolymer solution during 48 h. 150 μL of block copolymer solution without air bubbles was injected onto the lower plate of the cone-plate geometry using a syringe. In addition, a laboratory rheometer (RC20-CPS) with cone-plate geometry (plate diameter of 25 mm, cone angle of 1°) was used to measure the dynamic viscosity of PS<sub>84</sub>-*b*-P4VP<sub>16</sub><sup>197</sup> solutions in a mixture of DMF/THF at a ratio of 55/45 wt% versus shear rate. 80 μL of block copolymer solution without air bubbles was injected onto the lower plate of the cone-plate geometry using a

syringe. The rheological tests were immediately started after insertion of the sample in order to minimize the effect of solvent evaporation.

#### **2.4. Small-Angle X-ray Scattering (SAXS)**

SAXS measurements of the block copolymer solutions were performed at the BioSAXS beamline (P12) of PETRA III synchrotron storage ring at DESY, Hamburg. The solutions were injected into glass capillaries with a wall thickness of 10  $\mu\text{m}$  and a diameter of 1.5 mm by using a syringe with a needle diameter around 1 mm. The sample holder of the block copolymer solution was sealed with epoxy resin to prevent solvent evaporation during SAXS measurements. The beamline was configured with an X-ray wavelength  $\lambda=1.2407 \text{ \AA}$  corresponding to a photon energy of 10 keV. The sample-to-detector distance was 3068 mm which allowed SAXS data to be obtained in a  $q$  range from 0.06 to 0.4  $\text{nm}^{-1}$ . The magnitude of the scattering vector  $q$  is defined by  $q = 4\pi(\sin \theta)/\lambda$ , where  $\theta$  is half of the scattering angle.

#### **2.5. Hollow fiber membrane characterization**

The cross section and the surface morphology of the hollow fiber membranes were evaluated using scanning electron microscopy (SEM) (LEO 1550VP Gemini from Carl ZEISS) at a potential of 5 kV. The hollow fibers were freeze fractured in liquid nitrogen to preserve their microscopic morphology. The sample surface was sputter coated with a thin layer of Pt. Average pore sizes on the SEM micrographs were measured by the analySIS (Olympus) software.

#### **2.6. Permeance measurements**

The modules for the pure water flux measurement contained one fiber with an effective length of about 20 cm. For preparation of modules, the hollow fiber was inserted into a stainless steel tube sealed at both extremities by epoxy glue. Deionized water as feed solution was pumped through the lumen side of the module under 1 bar nitrogen pressure and permeate flow out from shell side of membrane module. The water permeance  $P$  was calculated using the equation

$$P = V/Atp \quad (1)$$

where  $V$  is the volume of the permeated water (L),  $A$  is the effective membrane surface area ( $\text{m}^2$ ) (based on the inner diameter of the hollow fiber),  $t$  is the time of solution collection (h) and  $p$  is the pressure applied to the hollow fiber membrane (bar). For each sample module, the water permeation

was measured within the first hour. The average permeance for three membranes was calculated and expressed in the water flux. The time stability of water flux was also measured. Pressure stability of the hollow fiber membranes was tested in a pure gas system under varying nitrogen pressure. Nitrogen gas is fed through the lumen side of the fibers. For checking reproducibility, the gas flux was also measured for 3 different modules of the same fiber batch. Nitrogen permeation experiments were carried out at room temperature around 30 min for each pressure.

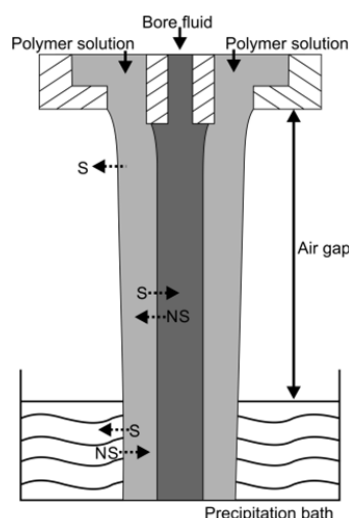


**Figure 1:** Schematic diagram of the dry-jet wet spinning process for preparation of PS-*b*-P4VP hollow fiber membranes. The solvent partially evaporates from the outer surface of the nascent hollow fiber causing a concentration gradient through the wall thickness of the fiber. The formation of hollow fiber is based on the non-solvent induced phase separation of polymer solution by rapidly exchanging the solvent with the non-solvent.

### 3. Results and discussion

#### 3.1. SAXS characterization

The state of a block copolymer solution prior to casting is a principal question in membrane casting, i.e. is there a self-assembled structure in solution before it is subjected to the casting procedure. Therefore, the structure of the spinning/casting solution in the equilibrium state was studied by SAXS. Previous researches on similar systems led to different conclusions. Phillip et al. developed a model assuming microphase separation during solvent evaporation in the cast solution to occur at the surface and then lead to a perpendicular orientation of microdomains, depending on the strength of solvent gradient, relaxation time of the polymer chains and the effective repulsive interaction between the dissimilar block segments [30]. Oss-Ronen et al. [15] investigated concentrated PS-*b*-

P4VP block copolymer solutions by cryo-SEM, cryo-TEM and small-angle neutron scattering. They conclude that micelles are present in these systems with the shorter P4VP block forming the core. In other works hexagonally packed micellar structures with the shorter P4VP blocks forming the corona were claimed. [12, 31-33].

Block copolymer micellization of two different PS-*b*-P4VP diblock copolymers in a mixture of DMF/THF at different polymer concentrations was analysed with synchrotron SAXS measurements. It is notable that for these diblock copolymers, well-ordered isoporous flat sheet membranes were achieved from solutions with an optimized concentration and evaporation time around 5-10 s after casting prior precipitation. In Figure 2(a), the SAXS scattering curve of the lowest concentration is dominated by a very broad weak peak which can be assigned to the correlation hole of a completely disordered block copolymer [34]. With increasing concentration, this broad peak becomes more prominent as the decreasing amount of the solvent mixture screens the repulsive interactions between dissimilar blocks less effectively. In consequence, the scattering maximum shifts to a lower  $q$  value of  $0.1152 \text{ nm}^{-1}$  at the highest concentration with a calculated  $(2\pi/q^*)$  long period of 54.5 nm. In addition, a less intense maximum appears at a higher  $q$  value, indicating some weak packing order. In fact, the results can indicate formation of liquid-like assembled micelles in solution with the average center-to-center distance of 54.5 nm between the nearest micelles at higher concentrations. By controlling the evaporation time, this concentration (25 wt%) led to successful SNIPS flat sheet membrane. During the evaporation time, the initially mostly disordered block copolymers start to self-assemble into ordered microdomains at the surface of the film due to the crossing of the concentration dependent disorder-order transition [30]. With increasing THF concentration and decreasing polymer concentration, the position of the dominant peak slightly shifts to lower  $q$  values which corresponds to an increase of the long period. The scattering profile at the highest concentration of the diblock copolymer with lower molecular weight and higher weight percentage of P4VP block shows the long period distance of 50 nm between the nearest micelles, see Figure 2(b). For this block copolymer, 26 wt% is a suitable polymer concentration for casting a homogeneous regular porous membrane. Recently, it was established that controlling self-assembly of the block copolymer micelles in solution is crucial in the final pore morphology formation of membranes [12, 31, 32]. However, the scattering patterns of the concentrated solutions do not clearly show the presence of hexagonal order. The SAXS results show that the suitable system for membrane formation (spinning /casting) is a block copolymer solution which is very close to the disorder-order

transition, i.e. a transition between a disordered phase or liquid-like assembled micellar structure to an ordered microphase separated structure. This is in agreement with SANS experiments on a similar system [15] and with dynamic light scattering data for another diblock copolymer solution [35]. A more detailed analysis of the structure formation of a block copolymer solution during evaporation of a fast and a slow evaporating solvent with different selectivities for the different blocks will be given elsewhere [36].

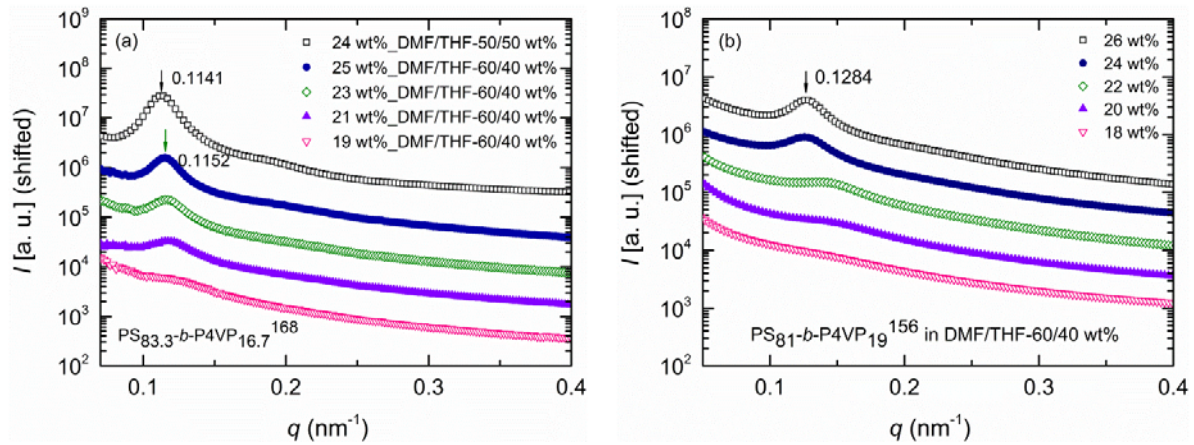


**Figure 2:** Scattering profiles of (a)  $\text{PS}_{83.3}\text{-}b\text{-P4VP}_{16.7}^{168}$  and (b)  $\text{PS}_{81}\text{-}b\text{-P4VP}_{19}^{156}$  solutions at various concentrations in mixtures of DMF/THF.

### 3.2. Rheological properties

Processing of PS-*b*-P4VP diblock copolymer solutions for preparation of hollow fibre membranes is strongly influenced by the rheological properties of the polymer solutions. Consequently, different rheological tests in shear were performed in order to investigate the flow properties of a PS-*b*-P4VP diblock copolymer solution. Rheological experiments in oscillation and in rotation were carried out in order to elucidate the transient response of the solutions and to determine their viscous and elastic properties. Several rheological tests were performed in order to characterize the rheological properties of the diblock copolymer solution. The time-dependent and the stationary shear viscosity were determined in stress-growth tests where the sample was sheared with a constant shear rate during a period of 100 s. Furthermore, rheological experiments in the oscillatory mode were performed. The sample was sheared at a constant angular frequency of  $\omega = 6.28$  rad/s. The shear amplitude changed alternately in intervals of 50 s starting with  $\gamma_0 = 10\%$  in the first interval of 50 s

and was increased up to 1000% in the second interval of 50 s. In the third interval, a shear amplitude of 10% was again chosen, etc. Amplitude sweeps at an angular frequency of  $\omega = 6.28$  rad/s with shear amplitudes in the interval from 0.1% to 1000% were also performed. First the shear amplitude was incrementally increased from 0.1% to 1000% and subsequently decreased from 1000% to 0.1%.

The results of the stress-growth tests are shown in Figures 3 and 4. Figure 3(a) presents the time-dependent viscosity for different shear rates. At low shear rates up to  $1 \text{ s}^{-1}$ , the transient viscosity increases with time. This effect is most probably caused by the effect of structure formation. At larger shear rates (equal or larger than  $10 \text{ s}^{-1}$ ) the viscosity attains a constant value. In addition, the start-up regime (increase of viscosity because of the viscoelasticity of the polymer solutions) is very short at shear rates equal or larger than  $10 \text{ s}^{-1}$ . At these shear rates (corresponding to large stresses), no effect of structure formation can be seen. Therefore larger stresses which are present in the shear flow in the spinneret prohibit structure formation of the sample in the spinneret.

Polymer solutions are characterized by a viscoelastic behaviour which implies a distribution of relaxation times after an imposed deformation. Figure 3(b) presents the time-dependent relaxation modulus  $G(t)$  which was calculated using the data in Figure 3(a) and the equation

$$\eta(t) = \int_0^t G(t') dt'.$$

The relaxation modulus  $G(t)$  strongly decreases with time and attains the slope -1 on a double-logarithmic scale which has been also observed for critical gels [37]. Generally, the decay of the relaxation modulus appears on a very short time scale. This effect indicates that the memory of the polymer solution with respect to the deformation history is very short. Consequently, the orientation of polymer chains in the spinneret can relax very rapidly.

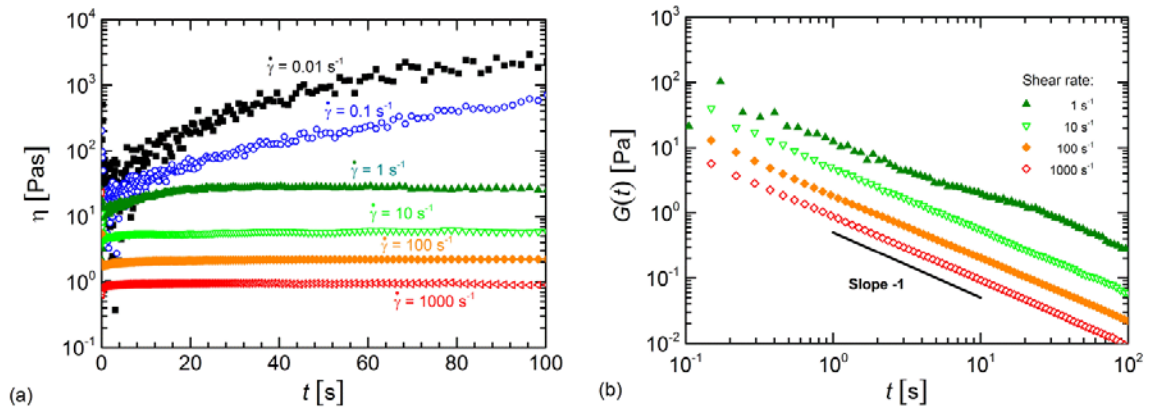


**Figure 3:** (a) Transient viscosity  $\eta(t)$  as a function of time  $t$  of 24 wt% PS<sub>83.3</sub>-*b*-P4VP<sub>16.7</sub><sup>168</sup> in DMF/THF 50/50 for different shear rates  $\dot{\gamma}$  at 25°C. (b) Relaxation modulus  $G(t)$  (derived using the data in (a)) as a function of time  $t$ . See text for details.

In Figure 4, the steady-state viscosity  $\eta_s$  of a similar diblock copolymer is shown as a function of shear rate  $\dot{\gamma}$  in the interval from 10 s<sup>-1</sup> to 3000 s<sup>-1</sup>. The steady-state viscosity  $\eta_s$  strongly decreases with shear rate. i.e. the polymer solution depicts a structure-viscous behavior. The behavior observed in Figure 4 appears to be not perfectly linear, so a power-law with the exponent -1/2 (as indicated by the dashed line) describes the measured data only insufficiently.

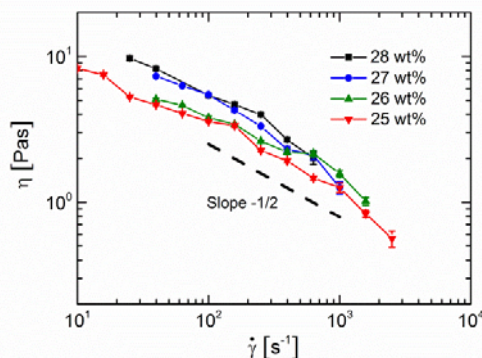


**Figure 4:** Stationary viscosity  $\eta_s$  as a function of shear rate  $\dot{\gamma}$  for PS<sub>84</sub>-*b*-P4VP<sub>16</sub><sup>167</sup> in DMF/THF 55/45 The measurement temperature was 25°C. Since the steady-state value could only be determined for shear rates equal or larger than 10 s<sup>-1</sup>, the shear rate range is limited to the interval from 10 s<sup>-1</sup> to 3000 s<sup>-1</sup>. The dashed line indicates a power-law behavior.

Rheological experiments in the oscillatory mode allow to determine the storage modulus  $G'$  and the loss modulus  $G''$ . The time-dependence of these moduli and possible irreversible phenomena were probed by oscillatory experiments with different shear amplitudes. The results of this experiment are shown in Figure 5. In the first interval, the shear amplitude was set to 10%. Both moduli attain large values and also increase with time which possibly results from the formation of a percolating structure (gel-like response). In the second interval the shear amplitude was set to 1000%. In the second interval, the moduli drastically decreased which indicates the almost instantaneously destruction of built-up structures. In the third interval, the shear amplitude was lowered again to 10%. The moduli increased again with time. This scenario of changing amplitudes and promptly changing moduli occurred several times which shows that the effect of increasing/decreasing moduli is reversible.

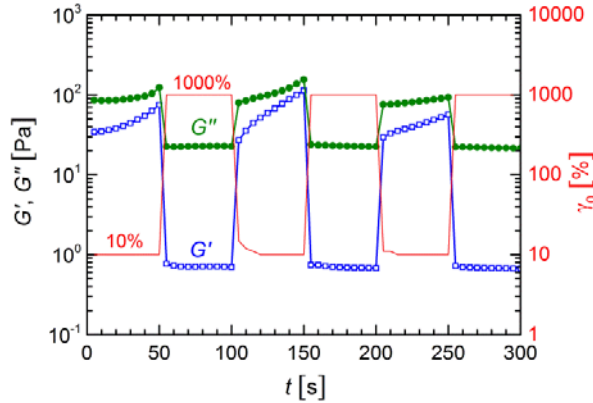


**Figure 5:** Storage modulus  $G'$  and loss modulus  $G''$  as a function of time  $t$  in oscillatory shear at constant frequency  $\omega = 6.28$  rad/s for 25 wt% PS<sub>83.3</sub>-*b*-P4VP<sub>16.7</sub><sup>168</sup> in DMF/THF 60/40. The shear amplitude was constant and equal to  $\gamma_0 = 10\%$  in the first interval of 50 s and equal to  $\gamma_0 = 1000\%$  in the second interval of 50 s. Then the shear amplitude alternately changed after 50 s.

To further explore the influence of shear on the disordered or very weakly microphase separated micellar structure of the PS-*b*-P4VP solutions, two separate experiments, namely the time-dependence and shear amplitude-dependence of  $G'$  and  $G''$  were performed at a constant frequency ( $\omega = 5$  rad/s). An example of the time-dependent behavior of the moduli at a constant low shear amplitude is presented in Figure 6. The time frame for the time sweep in Figure 6 is ten times larger than in Figure 5 in order to follow development of the dynamic moduli over a longer time. The increase of both storage and loss moduli indicates the formation of a gel in the block copolymer solution, as the initially more liquid like behavior ( $G'' > G'$ ) transforms into a state where  $G'$  and  $G''$  attain similar values. This is a typical feature of a percolating system (gel point) [37-39]. The percolating structure acts as a very weak reversible network leading to an enhancement of the moduli. A similar behavior was previously reported on block copolymer solutions under shear. Such solutions exhibit in the unperturbed state a viscos liquid-like behavior with  $G'' > G'$ . The cross-over of  $G'$  and  $G''$  is a hint of a thermoreversible gel formation with a more elastic behavior ( $G' > G''$ ) [38, 39].

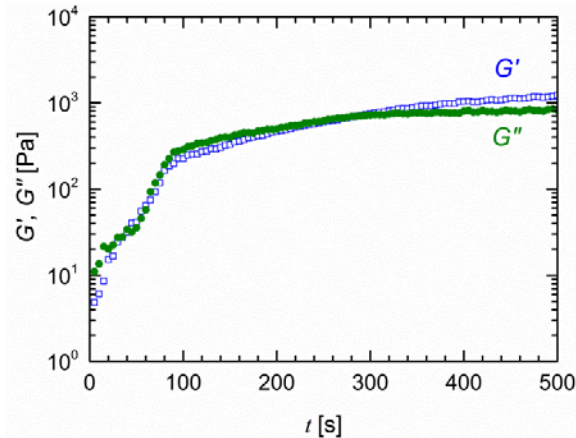


**Figure 6:** Storage modulus  $G'$  and loss modulus  $G''$  as a function of time  $t$  in oscillatory shear for 24 wt%  $\text{PS}_{83.3}\text{-}b\text{-P4VP}_{16.7}$  in DMF/THF 50/50 at constant frequency  $\omega = 5$  rad/s and shear amplitude  $\gamma_0 = 5\%$ .

In our experiments, a similar trend of  $G'$  and  $G''$  versus time was observed. The formation of a percolating structure as indicated by the cross over point occurred more rapidly at a shear amplitude of 5% compared to 10% shown in Figure 5. After approximately 100 s, the further, but significantly slower increase in  $G'$  indicates a further growth of the percolating structure, or possibly the disappearance of structural defects. The formation of the percolated structure is not very well defined, however, as there are two cross over points between  $G'$  and  $G''$ . After nearly 300 s the structure behaves more elastic at the angular frequency of 5 rad/s as  $G'$  is larger than  $G''$ . Up to this time both moduli attain rather similar values. This may reflect the onset and growth of percolating structures in the solution or gel. The structural change is also indicated by an increase in the viscosity at low shear rates, see Figure 3(a). The behavior of the moduli reveals that the solution concentration is near the concentration where a micellar network forms. As the increase of shear amplitude at constant frequency also implies an increase of shear rate, it can be expected that at higher shear rates, any thermoreversible network breaks up and polymer chains are elongated and oriented along the shear direction [40, 41] leading to shear thinning, cf. Figure 3(a).

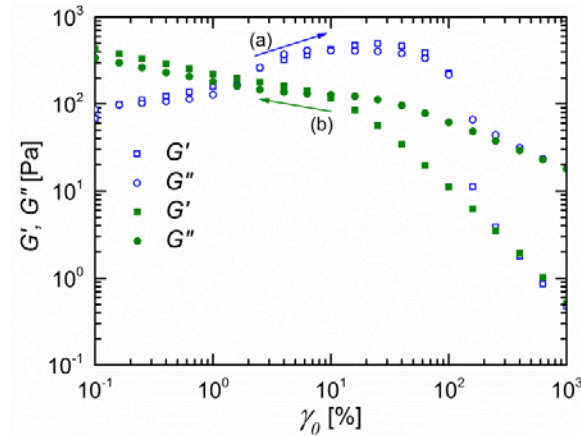


**Figure 7:** Storage modulus  $G'$  and loss modulus  $G''$  as a function of shear amplitude  $\gamma_0$  for 24 wt% PS<sub>83.3</sub>-*b*-P4VP<sub>16.7</sub><sup>168</sup> in DMF/THF 50/50 in oscillatory shear at constant frequency  $\omega = 6.28$  rad/s by sweeping from low to high shear strain and (b) from high to low shear strain.

The influence of increasing shear rate and deformation for the same system was studied by experiments with varying shear amplitude, see Figure 7. The shear amplitude was incrementally increased from 0.1% to 1000% and subsequently decreased to 0.1%. Note that the moduli change because of shear amplitude and measurement time. Initially at low shear amplitudes,  $G'$  and  $G''$  attain very similar values upon increasing the shear amplitude and attain a maximum at  $\gamma_0 \approx 20\%$  because of time-dependent structure-formation. The reversible network starts to decompose upon further increase of the shear amplitude until it transforms into a less elastic state at  $\gamma_0 \approx 100\%$  and becomes less viscous at higher shear amplitudes for the chosen frequency. As shown in Figure 3(a), the SAXS pattern of the equilibrium solution does not give evidence for a micellar lattice with any strong crystal-like ordering in the absence of shear flow. Thus, our rheological study on PS-*b*-P4VP solutions being suitable for fabricating asymmetric isoporous membranes do not agree with the rheological data and their interpretation published by Madhavan et al. [21]. They emphasized the strong contribution of the elastic modulus due to the effect of micellar assembly in solution, although no significant order was observed on the SEM micrograph of the resulting membrane surface. Our rheological experiments are in good agreement with the SAXS results and give no evidence for a well-ordered micellar assembly of the block copolymers in solution, although by appropriate tuning of the spinning conditions and the evaporation time, hollow fiber membranes with regular pores on the top surface were obtained from this solution.

### 3.3. Morphology of block copolymer hollow fiber membranes

In the first preparation of asymmetric PS-*b*-P4VP hollow fiber membranes, the SNIPS method was successfully applied to design a continuous permeable porous structure from micrometer-scale pore sizes to the self-assembled nanoscale pore sizes on the top surface of the fibers [29]. In a similar attempt, Hilke et al. [42] produced PS-*b*-P4VP hollow fibers by adjusting the solvent mixture to improve uniformity of the pore morphology and mechanical stability of the membranes. In the present study, we developed regularity of the hexagonally packed pore morphology by tuning the spinning conditions and PS-*b*-P4VP solution parameters. PS-*b*-P4VP diblock copolymers with different molecular weights and compositions were chosen to prepare the spinning solutions in a mixture of DMF/THF. The compositions and molecular weights of the block copolymers and also the solvent composition of DMF/THF were chosen in the ranges that were known to perfectly provide the desired integral asymmetric membranes with uniform nanostructure surface above a macroporous support layer in a flat sheet geometry [11]. Several experiments were carried out for each block copolymer to define the optimal solution concentration and solvent composition required for the fabrication of desired SNIPS flat sheet and hollow fiber membranes based on SEM results.

The rheological behavior of the optimized solutions under shear flow and SAXS traces of the investigated systems in equilibrium do not confirm micellar structure formation in the initial spinning/casting solution, as shown in the previous sections. However, the suitable concentration of initial solution required for periodic nanostructure formation on the membrane surfaces was found to be slightly below the disorder-order transition which makes the solution parameters sensitive to even small changes. As mentioned before, in these systems, THF is a good solvent for the PS blocks due to the solubility parameters, and much more volatile solvent compared to DMF, which is a good solvent for swelling the P4VP blocks [11-15]. Change of the solvent composition leading to the appropriate concentration during solvent evaporation drives the system to microphase separation and formation of micelles in solution. Consequently, orientation of the pore-forming domains into a hexagonal packing order propagates through the solvent evaporation process, as during evaporation gradients of both the solvent concentration and solvent composition are built up perpendicular to the surface.

In the dry/wet spinning process, in addition to the parameters discussed so far, the shear stress in the spinneret and in the spin line combined with the solvent and non-solvent exchange between the

flowing polymer solution and the bore fluid through the immediately solidified internal skin very likely influences the kinetics of block copolymer microphase separation. Shear thinning of the solution in the spinneret and gravity force in the air gap have a significant effect on the relaxation of the blocks at the die exit and on the kinetics of the self-assembly. The relaxation rate of the block copolymer chains is one important parameter in the formation process of integral asymmetric membranes [30] therefore not only is a function of concentration, but also of the effective mechanical deformation acting on the block copolymer polymer chains, which varies across the sheared cylindrical polymer solution. Although dimensions, stability and filtration performance of the resulting hollow fibers are affected by shear flow, the effect of the complex shear stress distribution in the spinneret and in the spin line on the viscoelastic behavior of the block copolymer solutions and micellar morphology still is not thoroughly understood. Hence, in order to reduce the effect of high shear stress on the micellar morphology and to avoid the break-up of the micelles, the spinneret used in our previous publication [29] was substituted by another one having a larger annular gap. All experiments were carried out at a short air gap (to minimize the effect of elongational stress outside of the spinneret) and water was chosen as coagulating bore fluid. Figure 8 shows the asymmetric continuous porous structure across the macrovoid free cross-section of the PS-*b*-P4VP hollow fiber membranes fabricated by the SNIPS process. The abbreviations of  $Q_p$ ,  $Q_b$  and  $L_{air}$  correspond to the polymer solution flow rate, bore fluid flow rate and air gap distance, respectively. Deformation of the pores shape from round shape to elliptical pores can be a result of the less relaxation of the shear-induced molecular orientation in the air gap followed by gravity force in the spin line and radial shrinkage of the hollow fibers due to the solvent non-solvent exchange through the solidification process.

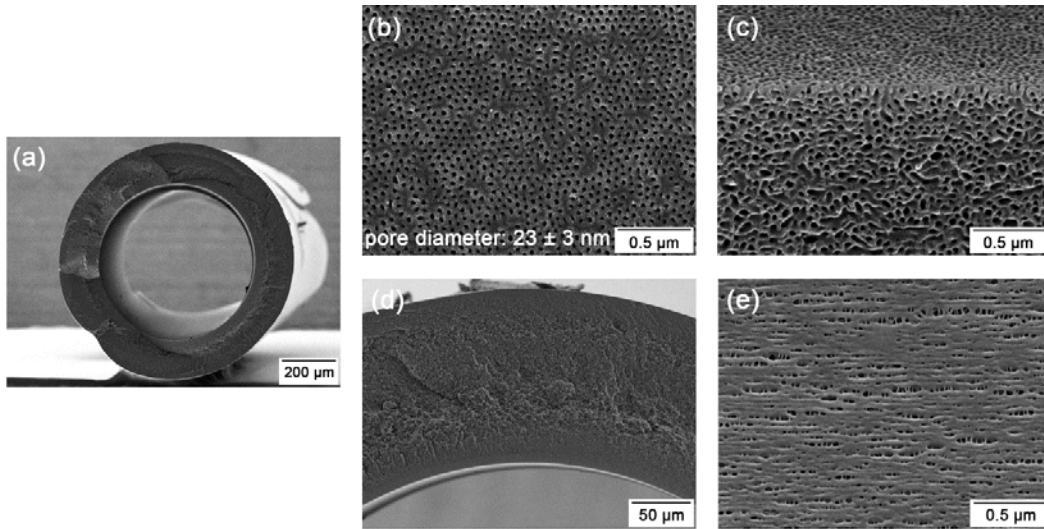


**Figure 8:** SEM micrographs of the hollow fiber membrane fabricated via the SNIPS process from 27 wt% solution of  $\text{PS}_{82.7}\text{-}b\text{-P4VP}_{17.3}$ <sup>154</sup> in the solvent mixture of DMF/THF 60/40 wt% at  $Q_p$ : 1.2 ml/min,  $Q_b$ : 0.6 ml/min and  $L_{\text{air}}$ : 10 cm. (a) Macrovoid free cross-section, (b) Top surface showing uniform periodic pores, (c) Cross-section near the surface showing extended pores in vertical direction above the disordered sponge-like macroporous matrix (d) Large view of cross-section and (e) Porous inner surface showing shear-induced oriented structure.

In fabrication of hollow fiber membranes by the SNIPS procedure, the spinning time between the spinneret and coagulation bath allows evaporation of the volatile solvent causing a concentration gradient perpendicular to the top outer surface of the fiber. Within an appropriate spinning time the concentration gradient through the wall thickness of the fiber can be developed with sufficient high concentration on the top surface to assemble the well-defined pore layer. Propagation of polymer concentration by the external solvent evaporation from the outer surface is combined with the simultaneous internal solvent non-solvent exchange. This occurs as the polymer solution comes into contact with the bore fluid at the die exit which also leads to shrinkage and rapid solidification of the inner surface. Some of the spinning parameters such as air gap, polymer solution flow rate and bore fluid flow rate tune the spinning time and among them air gap distance has a more prominent controlling effect. By optimizing these parameters, a suitable spinning time directs the self-assembly to form the uniform well-organized pores on the top surface of the fiber.

Several experiments were carried out to determine the optimum possible air gap by adjusting the other effective key parameters. We decreased the air gap distance to the possible minimum (1 cm) which allowed us to direct the fiber flow into the coagulation bath by controlling the polymer

throughput. The results showed that pore self-assembly on the fiber surface can take place even in a very short processing time compared to the flat membrane, see Figure 9. However, the non-uniform cross section morphology can be a result of the low mechanical stability of the low viscous skin when entering into the immersion bath in 1 cm air gap. An increase of the air gap increases the solvent evaporation and therefore will create a gel-like skin with higher mechanical stability which reduces or removes the non-uniformity of the outer surface skin. Hollow fibers with irregular or non-circular outer surface have previously been reported at a short air gap distance while deformation was eliminated by increasing the elongational stress in the air gap [26, 43]. On the other hand, increasing the air gap prevents the formation of uniform pores possibly due to the enlargement of evaporation time besides the effect of elongational stresses. Both parameters lead to an increasing relaxation time of the polymer chains. We found 10 cm as an optimal air gap distance for all experiments. Hence, we avoided to increase it more than that in order to decrease the gravity effect in addition to control the spinning time in the proper required scale for structure formation. The desired uniform nanoporous structure can be created at a spinning time significantly less than the evaporation time required for solution casting flat membranes. Consequently in fabrication of self-assembled block copolymer hollow fiber membranes, optimizing the polymer solution flow rate as well as the air gap distance provides the suitable conditions to form a hexagonally packed array of uniform pores on the top surface of the fiber.

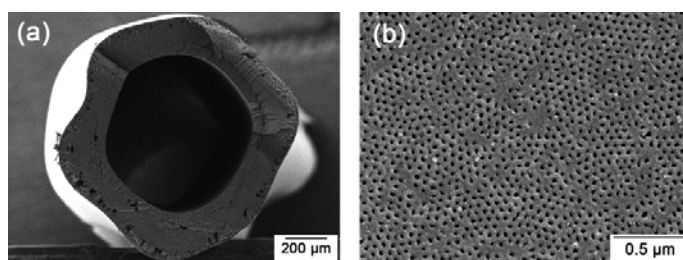
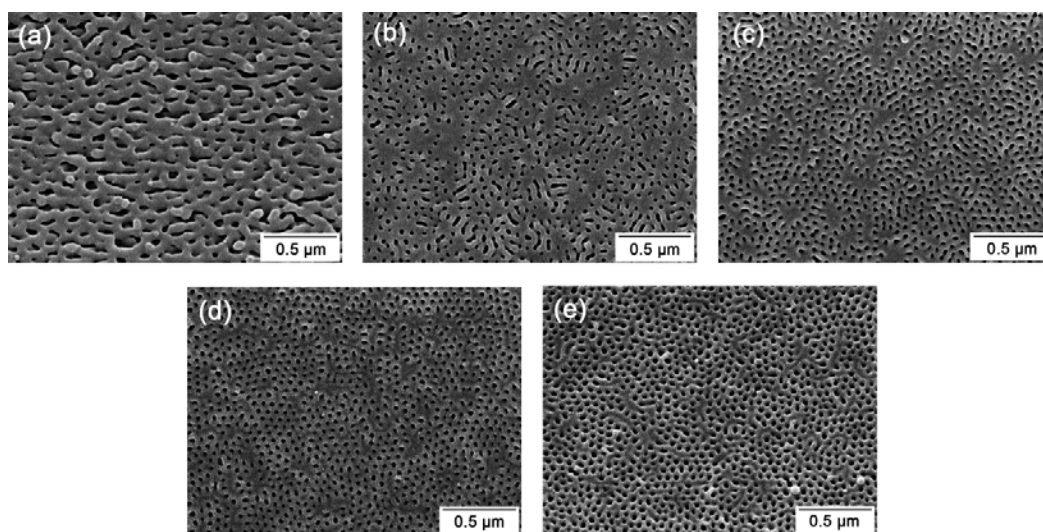


**Figure 9:** SEM micrographs of (a) the cross section and (b) the outer surface of the hollow fiber membrane fabricated from 27 wt% solution of  $PS_{82.7}\text{-}b\text{-}P4VP_{17.3}$ <sup>154</sup> in the solvent mixture of DMF/THF 60/40 wt% at  $Q_p$ : 1.4 ml/min,  $Q_b$ : 0.6 ml/min and  $L_{air}$ : 1 cm, spinning time was estimated less than 1 s.

In hollow fiber membrane formation, shear rate and stress within the spinneret and elongational stress in the spin line have a dramatical influence on the morphology, mechanical properties, and permeability and separation performance of the membranes [22, 23, 28]. The combination of shear rate in the spinneret and elongational stresses in the spin line causes orientation and stretching of the polymer chains and enhances the chain packing in the skin of hollow fiber membranes [28]. An

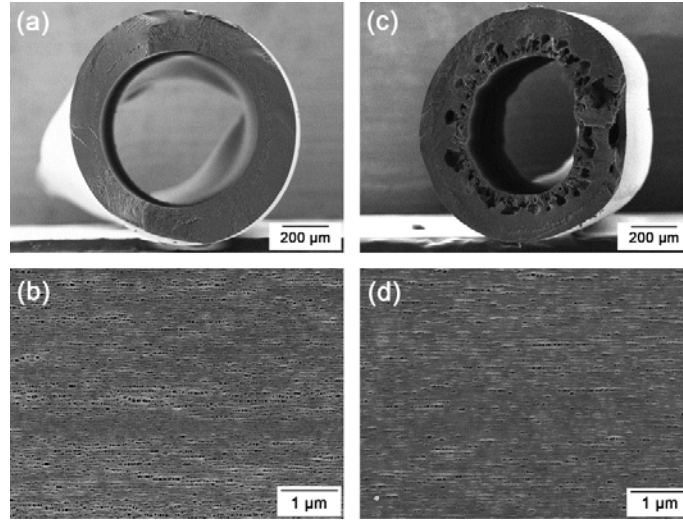
increase in the polymer solution flow rate leads to an increase of shear rate and prominently raises the shear stress at the spinneret wall. Increasing the shear stress causes a larger orientation of polymer chains and chain packing into a tighter skin structure. On the other hand, the strong dependence of the steady-state viscosity on shear rate depicts shear thinning of the block copolymer solutions. Consequently, the balance of these factors, shear-induced orientation, macromolecular-stretching induced by elongation and structure-viscous behavior, determine the molecular chain packing and relaxation rates of the blocks after spinneret exit in the air gap region. However, in the SNIPS process of block copolymers hollow fiber membranes, coupled effects of these parameters may significantly influence the kinetics of pore assembly and structure formation. In order to investigate the effect of these key parameters on the structure formation and fiber dimensions, we categorized our experiments into three groups: fabrication of hollow fibers by varying the polymer solution flow rate at constant bore fluid flow rate; varying the bore fluid flow rate at constant polymer solution flow rate; and varying the bore fluid and polymer solution flow rate to keep a constant ratio of these two flow rates.

Figure 10 shows the dependence of the uniformity of nanoscale pore formation on the outer surface of the membranes from the polymer solution flow rate. We started fiber spinning at very low polymer solution flow rate which lets us fabricate membranes at low shear rates as well. The polymer flow rate was varied (increased) while the bore fluid flow rate was kept constant. Since the axial velocities of both polymer solution and bore fluid flow change through the fiber traveling along the air gap region [44], see Figure 1, and solution velocities depend on the bore fluid flow rate, therefore the spinning time cannot be estimated precisely from the axial velocity of the polymer solution at the spinneret outlet. Consequently, the spinning time could be roughly measured for the nascent fiber falling into the coagulation bath without rolling up. For the spun fiber at  $Q_p$ : 1.2 ml/min,  $Q_b$ : 0.6 ml/min and  $L_{air}$ : 10 cm the spinning time was defined around 2-3 s.



**Figure 10:** SEM micrographs of the outer surface of the hollow fiber membranes spun from 27 wt% the solution of PS<sub>82.7</sub>-*b*-P4VP<sub>17.3</sub><sup>154</sup> in the solvent mixture of DMF/THF 60/40 wt% at  $Q_b$  : 0.6 ml/min,  $L_{air}$  10 cm and polymer flow rate of (a)  $Q_p$ =0.6 ml/min, (b)  $Q_p$ =0.8 ml/min, (c)  $Q_p$ =1 ml/min, (d)  $Q_p$ =1.2 ml/min and (e)  $Q_p$ =1.4 ml/min.

It was found that there is a critical polymer solution flow rate below which the periodic pores are not uniformly assembled on the top surface. It can be a result of the spinning time and moreover the shear flow rate within the spinneret. The shear rate is controlled by both spinneret die gap and polymer solution flow rate. Depending on the block copolymer solution parameters, the shear rate requires a lower extreme limit for the structure formation. In fact, the shear flow in the spinneret as an external force can promote packing of the well-ordered structure faster and decline the required evaporation time. Since at low polymer throughput the polymer solution stays longer in the spinneret die, more alignment can occur and result in a longer relaxation time after the polymer comes out of the spinneret. Increasing the polymer flow in the spinneret increases the tendency of the polymer solution to fast relaxation of chains at the die exit. Thus, after leaving the spinneret, fast enough relaxation of the shear-induced oriented chains compared to the spinning time scale (related to the polymer flow rate) accelerates lattice formation of the hexagonally packed cylinders on the top layer skin perpendicular to the hollow fiber axis. Our results confirm that in the SNIPS process of hollow fiber compared to the flat sheet membrane, the concentrated solution requires lower processing time for kinetic trapping of the ordered domains during solvent removal. Therefore, the spinning time requires tuning in order to prevent the transition from a metastable to a closer to equilibrium structure in the air gap region.



**Figure 11:** SEM micrographs of the hollow fiber membranes fabricated from the 27 wt% solution of PS<sub>82.7</sub>-*b*-P4VP<sub>17.3</sub><sup>154</sup> in the solvent mixture of DMF/THF:60/40 wt% at  $Q_b$ : 0.6 ml/min and  $L_{air}$  10 cm. From left to right, (a) and (b) the cross section and inner surface at  $Q_p$ : 0.6 ml/min, (c) and (d) the cross section and inner surface at  $Q_p$ : 2 ml/min.

In hollow fiber spinning processes, the extrusion of the viscous polymer solution is associated with a wide range of shear stress when it flows through the winding channels within a spinneret [23]. However, at the end of the spinneret we mainly have a shear flow for a very short time followed by a very quick exposure to the non-solvent quench bath. In all sets of our spinning experiments, even at lowest applied polymer solution flow rate the maximum shear rate at the wall of the spinneret was estimated higher than  $100 \text{ s}^{-1}$ , using the equation for Newtonian viscosity behavior [45]

$$\dot{\gamma} = \frac{8 Q_p}{\pi} \frac{1}{(R_2^2 - R_1^2)^2 / \ln(R_2/R_1) - (R_2^4 - R_1^4)} \left( \frac{r}{2} + \frac{(R_2^2 - R_1^2)}{4r \ln(R_2/R_1)} \right)$$

where  $\dot{\gamma}$  is the shear rate at the wall in the annular spinneret,  $Q_p$  is the polymer solution flow rate,  $R_i = d_i/2$  and  $R_o = d_o/2$  are inner and outer radii. The position  $r$  is given by  $R_i$  and  $R_o$ , respectively. Our rheological experiments reveal that even if a micellar assembly exists in the solution or the structure initiates ordering at low shear strain, it will be broken up at high shear rate at the end of the spinneret. On the other hand, due to the short relaxation times in polymer solution, the polymer blocks rapidly relax at the exit of spinneret. This fast molecular relaxation takes place accompanied with the solvent evaporation at the outer surface of the fiber in the air gap. As also indicated by the  $G'$  and  $G''$  curves versus strain amplitude in Figure 7, decreasing the shear rate from higher to the lower strain led to a

build-up of the storage and loss moduli and a cross over at lower strain which indicates the build-up of a structure. In fact, decreasing shear may allow the broken-up structure to reassemble again very fast to a gel-like structure. The conditions are rather similar in the dry/wet spinning process of block copolymer solutions. Partial release of the shear stress in the air gap region resembles decreasing the shear rate from higher to the lower strain which can be a driving force to develop the block copolymer self-assembly, see also the experiments in Figure 5. Although it was not possible to control easily the fiber flow into the precipitation bath at high polymer solution throughput and short air gap, however, it was attempted to avoid applying high polymer solution flow rate as high shear flow can significantly change the structure or the solution.

Besides the shear-induced homogenisation of mixtures, however, the shear-induced inhomogeneity in polymer solutions is also possible. Shear-induced phase separation (SIPS) into polymer rich and polymer poor regions has been reported for semidilute solutions of some polymers in marginal or theta-solvents [46-51]. In hollow fiber spinning process, besides thermodynamics of the polymer solution the external forces can also affect the phase behaviour and structure evolution. Phase inversion process usually occurs non-isothermally under tension or elongational stress in the air gap distance and lead to a change of the conformational entropy induced by these stresses [2, 52, 53]. Therefore, besides the influence of the external field on the miscibility of the block copolymer with the solvent, it also may influence the microphase separation of the block copolymer itself [54]. Furthermore these effects are coupled with the selectivity of the different blocks to the different components of the solvent mixture. Therefore solution parameters such as concentration and solvent composition require adjustment due to the different selectivity of the solvents leading to different relaxation rate of the blocks.

The impact of a spatially non-uniform stress field makes the structure formation in hollow fiber membranes more complex compared to flat sheet membranes. In hollow fiber spinning via the SNIPS process formation of the outer shell side by solvent evaporation simultaneously occurs with the internal non-solvent diffusion/precipitation on the lumen side which stabilizes the spinning line. Cylindrical geometry of the fiber accelerates diffusion flow in the radial direction toward the center because of the different chemical potentials in the polymer solution and bore liquid. Prior to the immersion bath, solvent is driven to diffuse from the polymer solution into the bore fluid due to the lower chemical potential and difference in solubility parameters. Therefore, in addition to evaporation of the volatile solvent from the outer layer in the air gap, rapid solvent migration into the

bore fluid from the inner wall can influence the polymer concentration gradient over the cross section of the fiber. In other words, simultaneously with the solvent concentration gradient in perpendicular direction to the outer surface due to the solvent evaporation, there is an effect of the water concentration gradient in perpendicular direction to the inner surface resulting from water diffusion. A fast enough rate of the solvent removal at the top surface of the fiber due to the coupling effects of solvent evaporation and migration can enhance the periodic pore formation in a very short spinning time.

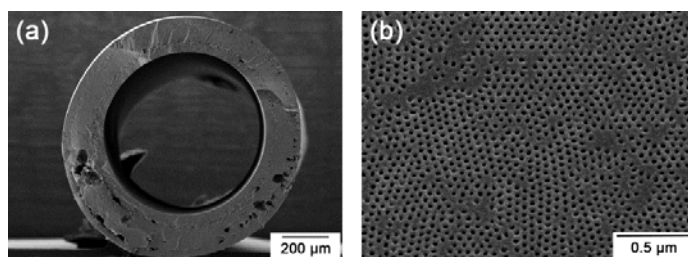


**Figure 12:** SEM micrographs of (a) the cross section and (b) the outer surface of the hollow fiber membranes spun from 25 wt% solution of  $PS_{83.3}\text{-}b\text{-}P4VP_{16.7}$ <sup>168</sup> in the solvent mixture of DMF/THF 60/40 wt% at  $Q_p$ : 4 ml/min,  $Q_b$ : 2.4 ml/min and  $L_{air}$  10 cm.

In a dry/wet spinning process, the overall cross-section morphology of the hollow fiber is greatly influenced by the spinneret shear-induced orientation along with the molecular relaxation in the air gap and also by the bore fluid flow rate. Therefore, in addition to see the effect of shear rate on the self-assembly of periodic pores on top surface, the cross section and inner surface morphologies of the hollow fibers were examined by analyzing the SEM micrographs. Figure 11 presents the cross-section and inner surface morphology of the membranes spun at different polymer solution flow rates with a constant bore fluid flow rate. Clearly, one can see the effect of shear stresses on the fiber cross-section and inner surface morphology. The shear-induced molecular orientation within the spinneret was rapidly frozen into the solidified dense skin once the polymer solution comes into contact with the bore fluid. The inner surface morphology resembles the parallel distribution of the closely-packed nanofibers/nanonodule aligned into the fiber axis direction. Although the structural orientation of the inner surface is highly visible in the nodular direction, the irregular nanometer-scale pores were formed among the nodular structure due to the non-solvent diffusion in the internal coagulation process. By increasing the polymer solution flow rate at constant bore fluid flow rate, the rate of inner skin formation and solidification is variable due to the nonconstant rate of solvent/non-solvent exchange. In addition, the higher shear flow (or higher ratio of the polymer solution flow rate

to the bore fluid flow rate) enhances the molecular orientation to the further close packing of the nanonodule structure and merges them to the tighter structure with the smaller pore size and denser skin. Obviously, the morphology and porosity of the rapidly formed selective inner skin significantly has influence on the water flux permeation and selectivity.

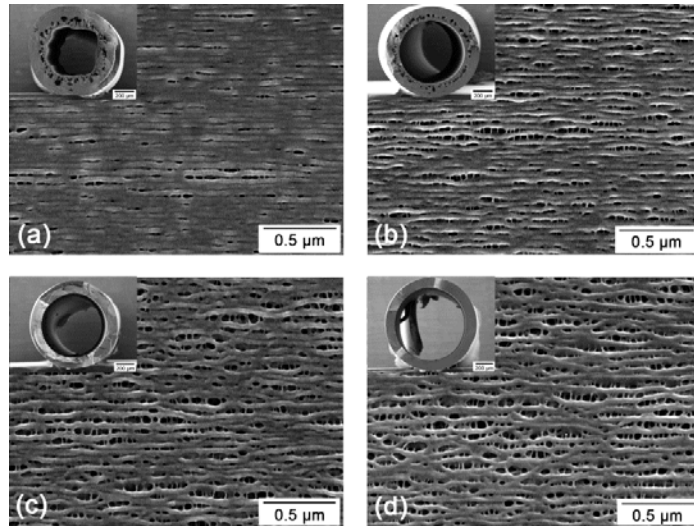


**Figure 13:** SEM micrographs of the inner surface and cross-section of the hollow fiber membranes spun from 27 wt% solution of PS<sub>82.7</sub>-*b*-P4VP<sub>17.3</sub><sup>154</sup> in the solvent mixture of DMF/THF 60/40 wt% at  $Q_p$ : 1.4 ml/min,  $L_{air}$  10 cm and different (a)  $Q_b$ : 0.4 ml/min, (b)  $Q_b$ : 0.8 ml/min, (c)  $Q_b$ : 1.2 ml/min and (d)  $Q_b$ : 1.6 ml/min.

At low polymer solution flow rate, the hollow fiber membranes also exhibit a quite uniform cross-section consisting of sponge-like structures at both edges of the fibers, see Figure 11. By increasing the polymer solution throughput, the cross-sectional view presents an asymmetric structure including some drop-shaped macrovoids developed within the sponge-like supporting structure. The cross-section of the hollow fiber shows non-uniform wall thickness with a wavy/deformed bore channel. The irregularity of the hollow fiber on the lumen side is strongly affected by the too low flow of the bore fluid. These defects can lead to mechanical failure if the hollow fiber is operated at high pressure [2]. Deformation of the inner layer can be fully removed by increasing the bore fluid flow rate or in fact simultaneously increasing polymer solution and bore fluid flow rate while maintaining a constant ratio between them. By increasing the bore fluid volume, the lumen irregularity is minimized due to the higher pressure in the inner contour. The experimental results confirmed that the higher bore fluid flow rate or in fact higher ratio of the bore fluid flow rate to the polymer

solution flow rate particularly at higher polymer flow rates can avoid non-uniformity of the cross section or deformation of the inner layer, see Figure 12.

The hollow fibers with smaller thickness result from the higher bore fluid flow rate which assists the formation of the macrovoid free structure, see Figure 13. In addition, the bore fluid flow rate controls the inner skin morphology and porosity which can play an important role in the hollow fiber separation and permeance. Higher pressure on the inner skin due to the higher velocity of the bore fluid disorients the close-packed nanonodule structure and leads to the looser structure with larger pore size and higher porosity. Our results prove that, by selecting the suitable ratio of the bore fluid flow rate to the polymer solution flow rate, besides assembling the selective uniform pores layer on the top surface, it also provides the regular shape of hollow fiber membranes from different block copolymer solutions (Figure 14). The hollow fiber membrane obtained by SNIPS show a smaller average pore size compared to the flat sheet membrane cast with the similar block copolymers [11]. The hollow fiber which was fabricated from a block copolymer with a higher total molecular weight and lower P4VP weight ratio displays a larger average pore diameter compared to the spun fiber from a block copolymer with lower total molecular weight and higher P4VP weight ratio.

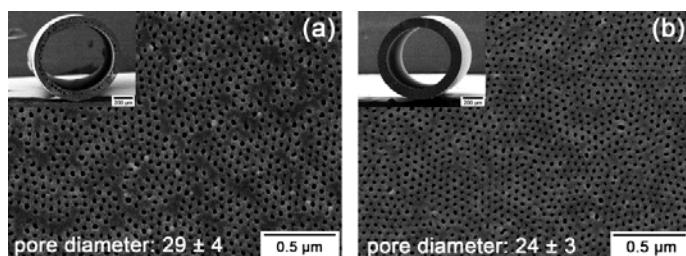


**Figure 14.** SEM micrographs of the outer surface and average pore diameter of the hollow fiber membranes spun from (a) 24 wt% solution of  $PS_{83.3}\text{-}b\text{-}P4VP_{16.7}^{168}$  in the solvent mixture of DMF/THF 60/40 wt% and (b) 25 wt% solution of  $PS_{81}\text{-}b\text{-}P4VP_{19}^{156}$  in the solvent mixture of DMF/THF 50/50 wt% at optimized spinning parameter ( $Q_p$ : 1.8 ml/min,  $Q_b$ : 1.2 ml/min and  $L_{air}$ : 10 cm).

### 3.3 Hollow fiber dimensions

In a dry-jet wet spinning process, dimensions of the hollow fibers strongly depend on the air gap distance and both polymer solution and bore fluid flow rate. In our experiments, in order to reduce the elongational effects on the structure formation and to control the processing time, the air gap distance was fixed in all experiments whereas the polymer solution flow rate and bore fluid flow rate were varied. However, in all experiments the outer diameters of the spun fibers were smaller than the outer diameter of the spinneret. This is caused by the more dominant effect of gravity force compared

to the extrudate-swell in the air gap. Figures 15(a) and (b) show the ratio of the inner diameter of the fiber to the inner diameter of the spinneret ( $\delta_1$ ), and the ratio of the wall thickness of the fiber to the annular gap of the spinneret ( $\delta_2$ ) under different spinning conditions. In the range of the applied polymer solution flow rates, the effect of increasing throughput on the inner diameter and wall thickness of the fiber are not distinct particularly at a low bore fluid flow rate. In addition, we cannot follow a special trend in dimensional changes as the deformed inner layer contour of the hollow fibers spun from the non-proper ratio of the polymer solution and bore fluid flow rate did not allow precisely to determine the fiber dimensions. At higher bore fluid flow rate,  $\delta_1$  is significantly higher than 1 which shows that the inner diameters of the hollow fibers are larger than the inner diameter of the spinneret. By increasing the polymer solution flow rate, because of the faster decrease in the inner diameter (less drag force and pressure on the inner layer) than in the outer diameter of the fibers,  $\delta_2$  rises due to the increase in the wall thickness of the fibers.

However, the bore fluid flow rate evidently plays a very significant influence on the cross-section area of the nascent fibers. The inner diameter of the dry-jet wet-spun fibers increases with an increase of bore fluid flow rate while the wall thickness decreases. This effect results from the faster increase of the inner diameter than of the outer diameter. Previous studies revealed that an increment in the bore fluid flow rate leads to an increase of the radial velocity and thus to a higher pressure on the lumen side. This effect causes the formation of a larger diameter [24, 27]. Furthermore, increasing the bore fluid flow rate increases the pressure on the inner layers of the hollow fiber membranes, which elongates and stretches the nascent fibers and leads to reduction of their thicknesses [55].

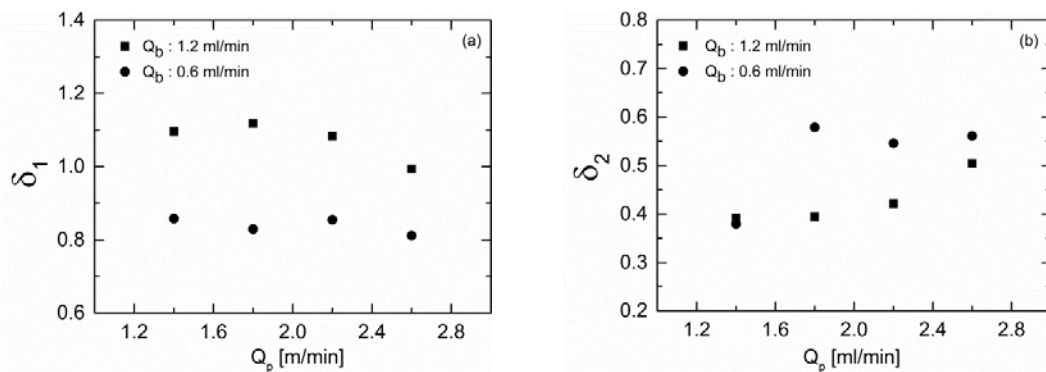


**Figure 15:** Hollow fiber membranes spun from the 25 wt% solution of  $PS_{83.3}\text{-}b\text{-}P4VP_{16.7}$  in the solvent mixture of DMF/THF 60/40 wt% at  $L_{air} : 10$  cm (a): ratio of the inner diameter of the fiber to the inner diameter of the spinneret ( $\delta_1$ ) and (b): ratio of the wall thickness of the fiber to the annular gap of the spinneret ( $\delta_2$ ) as a function of  $Q_p$  and  $Q_b$ .

### 3.4 Water Flux and gas pressure stability

Block copolymer membranes with high porosity and homogeneous pore size indicate remarkable potential as efficient and highly selective separation membranes [11, 56]. Our results reveal that the SNIPS procedure is capable to fabricate hollow fiber membranes with regular pore size in nanometer scale on the top outer surface. However, water flux of the PS-*b*-P4VP hollow fiber membranes correlates very well with the pore structure formation tailored by the SNIPS process due to the spinning conditions. Highly oriented and tightly packed structure of the inner selective layer has a negative influence on pure water permeation flux compared to the flat sheet membranes. To increase the water permeance, the porosity of the inner skin can be also improved by the bore fluid flow rate (see Figure 13) in addition to the solvent/non-solvent activity of the bore fluid [42].

An average initial water flux of around  $321 \pm 25 \text{ L m}^{-2} \text{ h}^{-1} \text{ bar}^{-1}$  was measured for the asymmetric isoporous PS<sub>83.3</sub>-*b*-P4VP<sub>16.7</sub><sup>168</sup> hollow fiber membrane with average pore size of 29 nm. In our work, the pure water flux is significantly higher in comparison with the value previously reported [42]. This improvement can originate from different reasons like cross-section structure, porosity and resistance effect of the inner selective layer as a result of the dissimilarity in the spinning conditions in addition to the solution parameters. Under constant pressure, the slight decline in the membrane water flux with time can be an effect of the smaller pore size due to the gradually swelling P4VP block inside the pore channels, see Figure 16 (a). In a previous study on similar PS-*b*-P4VP flat sheet membranes with average pore sizes of 25 and 38 nm, the maximum pure water flux was reported around 450 and 625  $\text{L m}^{-2} \text{ h}^{-1} \text{ bar}^{-1}$ , respectively [11]. Therefore, by controlling the spinning parameters and tailoring the hollow fiber morphology, pore size and porosity, and decline the resistance effect of the relatively close-packed structure of the inner surface, the water flux measurements can become comparable with the flat sheet membranes. The pressure stability of the mentioned membrane was tested by nitrogen gas permeation. These tests may provide information on its mechanical stability behavior of the fibers at elevated pressure. The hollow fiber was stable up to 11 bar pressure, see Figure 16(b). An increase of gas permeance as a function of pressure can be due to the elastic deformation (stretching) of fiber and the increase of pore diameter. The hollow fibers show viscoelastic properties at these elevated pressures which allow dimensional changes under pressure and dimensional regeneration under unstressed conditions.

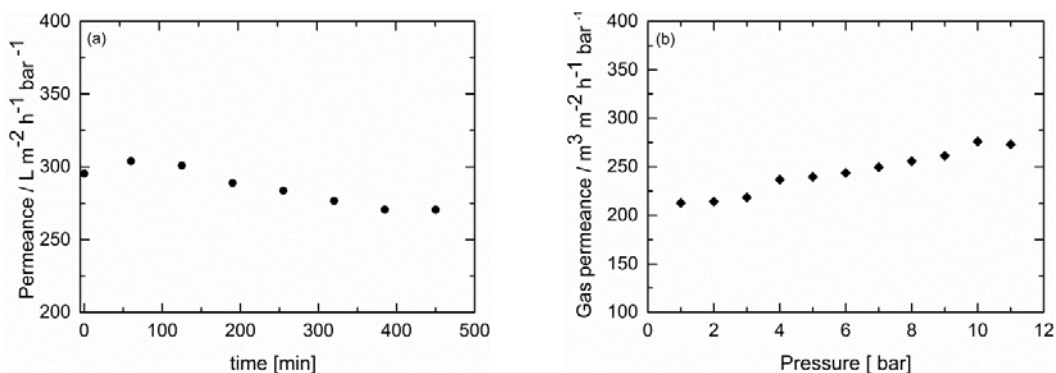


**Figure 16:** An example of the (a): time dependence of water flux and (b) gas pressure stability of the hollow fiber membrane spun from the 24 wt% solution of PS<sub>83.3</sub>-*b*-P4VP<sub>16.7</sub><sup>168</sup> in the solvent mixture of DMF/THF 50/50 wt% at  $Q_p$ : 1.4 ml/min,  $Q_b$ : 1.2 ml/min and  $L_{air}$ : 10 cm.

## Conclusion

Asymmetric PS-*b*-P4VP hollow fiber membranes with a nanometer scale-pore layer on the top surface were successfully fabricated via the well-known dry-jet wet spinning process. The uniform periodic pores were assembled above an asymmetric macroporous support layer by combination of the self-assembly and non-solvent induced phase separation of diblock copolymers (SNIPS). Our works focused on tailoring of the solution concentration, solvent composition as well as some important spinning parameters such as bore fluid flow rate, polymer solution flow rate and size of air gap. We analyzed our experimental observations by SEM micrographs and then modified the important parameters to assemble uniform well-organized pores on the surface as well as to achieve regular well-formed cross-section hollow fibers. Our focus also was on understanding the rheological behavior of the block copolymer solutions under shear flow. At low shear amplitudes, both  $G'$  and  $G''$  increase with time possibly resulting from formation of a gel-like structure. At large shear amplitudes, both moduli drastically decrease which indicates destruction of the built-up structures. SAXS measurements were carried out to investigate the structural features of the block copolymer solutions. The scattering profiles of the optimal solutions confirm that the starting point of membrane formation is a disordered or very weakly segregated micellar block copolymer solution. In addition, the membranes show a good water flux compared to previous results and also display a good stability under high pressure conditions.

## Acknowledgment

The authors are grateful to Brigitte Lademann for synthesizing the block copolymers and Ivonne Ternes for the rheological experiments. Anne Schroeder and Sofia Dami are acknowledged for their help with SEM investigations. Parts of this research were carried out at the light source PETRA III at DESY, a member of the Helmholtz Association (HGF). We would like to thank Vasyi Garamus for assistance in using beamline P12.

## References:

1. Bonyadi S, Chung TS, Krantz WB. *J. Membr. Sci.* 2007; 299: 200–10.
2. Peng N, Widjojo N, Sukitpaneelit P, Teoha MM, Glenn Lipscomb G, Chung TS, Lai JY. *Prog. Polym. Sci.* 2012; 37:1401–24.
3. Ho WSW, Sirkar KK, editors. *Membrane handbook*. New York: Van Nostrand Reinhold; 1992.
4. Matsuura T, editor. *Synthetic membranes and membrane separation process*. Boca Raton, FL, USA: CRC Press; 1994.
5. Nunes SP, Peinemann K-V, editors. *Membrane technology in the chemical industry*. 2nd ed. Weinheim, Germany: Wiley-VCH; 2006.
6. Peinemann K-V, Abetz V, Simon PF. *Nat. Mater.* 2007;6:992-6.
7. Schacher F, Ulbricht M, Muller AHE. *Adv. Funct. Mater.* 2009; 19 (7):1040–45.
8. Phillip WA, Dorin RM, Werner J, Hoek EMV, Wiesner U, Elimelech M. *Nano Lett.* 2011; 11 (7): 2892–2900.
9. Gu Y, Dorin RM, Wiesner U. *Nano Lett.* 2013;13:5323–28.
10. Dorin RM, Sai H, Wiesner U. *Chem. Mater.* 2013.
11. Rangou S, Buhr K, Filiz V, Clodt JI, Lademann B, Hahn J, Jung A, Abetz V. *J. Membr. Sci.* 2014; 451:266-75.
12. Nunes SP, Sougrat R, Hooghan B, Anjum DH, Behzad AR, Zhao L, Pradeep N, Pinnau I, Vainio U, Peinemann K-V. *Macromolecules* 2010;43:8079-85.
13. Nunes SP, Karunakaran M, Pradeep N, Behzad AR, Hooghan B, Sougrat R, He H, Peinemann K-V. *Langmuir* 2011;27:10184-90.
14. Nunes SP, Behzad AR, Hooghan B, Sougrat R, Karunakaran M, Pradeep N, Vainio U, Peinemann KV. *ACS Nano* 2011;5: 3516-22.
15. Oss-Ronen L, Schmidt J, Abetz V, Radulescu A, Cohen Y, Talmon Y. *Macromolecules* 2012;45: 9631-42.
16. Nunes SP, Car A. *Ind. Eng. Chem. Res* 2013;52: 993-1003.
17. Hahn J, Filiz V, Rangou S, Lademann B, Buhr K, Clodt JI, Jung A, Abetz C, Abetz V. *Macromol. Mater. Eng.* 2013.

18. Gallei M, Rangou S, Filiz V, Buhr K, Bolmer S, Abetz C, Abetz V. *Macromol. Chem. Physic.* 2013;214: 1037-46.
19. Clodt JI, Rangou S, Schroder A, Buhr K, Hahn J, Jung A, Filiz V, Abetz V. *Macromol. Rapid. Comm.* 2013; 34: 190-4.
20. Clodt JI, Filiz V, Rangou S, Buhr K, Abetz C, Höche D, Hahn J, Jung A, Abetz V. *Adv. Funct. Mater.* 2013;23:731-38.
21. Madhavan P, Peinemann K-V, Nunes SP. *ACS Appl. Mater. Interfaces* 2013.
22. Chung T-S, Teoh SK, Lau WWY, Srinivasan MP. *Ind. Eng. Chem. Res.* 1998; 37: 3930-38.
23. Chung T-S, Qin J-J, GU J. *Chem. Eng. Sci.* 2000; 55: 1077-91.
24. Qin J-J, Chung T-S. *J. Membr. Sci.* 2004; 229:1-9.
25. Ismail AF, Mustaffar MI, Illias RM, Abdullah MS. *Sep. Purif. Technol.* 2006; 49:10-19.
26. Widjojo N, Chung T-S. *T Ind. Eng. Chem. Res.* 2006; 45:7618-26.
27. Shen X, Zhao Y, Zhang Q, Chen L. *J. Polym. Res.* 2013; 20:136.
28. Feng CY, Khulbe KC, Matsuura T, Ismail AF. *Sep. Purif. Technol.* 2013;111: 43-71.
29. Radjabian M, Koll J, Buhr K, Handge UA, Abetz V. *Polymer* 2013;54:1803-12.
30. Phillip WA, Hillmyer MA, Cussler EL. *Macromolecules* 2010;43: 7763-70.
31. Dorin RM, Marques DS, Sai H, Vainio U, Phillip WA, Peinemann K-V, Nunes SP, Wiesner U. *ACS Macro. Lett.* 2012; 1: 614-17.
32. Marques DS, Vainio U, Chaparro NM, Calo VM, Bezhad AR, Pitera JW, Peinemann K-V, Nunes SP. *Soft. Matter.* 2013;9: 5557-64.
33. Marques DS, Dorin RM, Wiesner U, Smilgies D-M, Behzad AR, Vainio U, Peinemann K-V, Nunes SP. *Polymer* 2013.
34. Leibler L. *Macromolecules* 1980; 13: 1602-17
35. Hahn J, Filiz V, Rangou S, Clodt J, Jung A, Buhr K, Abetz C, Abetz V. *J. Polym. Sci. Polym. Phys.* 2013; 51:281-90.
36. Stegelmeier C, Filiz V, Abetz V, Perlich J, Fery A, Ruckdeschel P, Rosenfeldt S, Förster S, *Macromolecules*, submitted.
37. Mours M, Winter HH. *Adv. Polym. Sci.* 1997; 134: 165 -234.
38. Heinzer MJ, Han S, Pople JA, Martin SM, Baird DG. *Polymer* 2012; 53:3331-40.
39. Buitenhuis J, Förster S. *J. Chem. Phys.* 1997;107: 262-72.
40. Rychkov I. *Macromol. Theory. Simul.* 2005; 14: 207-42.
41. Rychkov I, Yoshikawa K. *J. Chem. Phys.* 2004; 120:3482-88.
42. Hilke R, Pradeep N, Madhavan P, Vainio U, Behzad AR, Sougrat R, Nunes SP, Peinemann K-V. *Appl. Mater. Interfaces* 2013; 5: 7001-06.
43. Zhang X, Wen Y, Yang Y, Liu L. *J. Macromol. Sci. Part B* 2008;47:1039-49.

44. Aroon MA, Ismail AF, Montazer-Rahmati MM, Matsuura T. *J. Membr. Sci.* 2010; 348: 13–20.
45. Shilton SJ. *J. Appl. Polym. Sci.* 1997; 65: 1359 -62,
46. Helfand E, Fredrickson GH. *Phys. Rev. Lett.* 1989: 62; 2468-71.
47. Yanase H, Moldenaers P, Mewis J, Abetz V, van Egmond J, Fuller GG. *Rheol. Acta.* 1991; 30:89-97.
48. Onuki, A. *J. Phy.: Condens. Matter.* 1997: 9, 6157.
49. Migler K, Liu CH, Pine DJ, *Macromolecules* 1996: 29; 1422-32.
50. Tan H, Watanabe H, Matsumiya Y, Kanaya T, Takahashi Y. *Macromolecules* 2003; 36: 2886-93.
51. Schubert B A, Wagner N J, Kaler E W, *Langmuir* 2004: 20: 3564-73.
52. Chung TS. *J. Membr. Sci.* 1997; 126:19–34.
53. Wolf BA. *Pure & Appl. Chem.* 1997; 69: 929-33.
54. Marques CM, Cates ME. *J. Phys. France* 1990; 51: 1733-47
55. Feng CY, Khulbe KC, Chowdhury G, Matsuura T, Sapkal VC. *J. Membr. Sci.* 2001; 189:193–203.
56. Hahn J, Clodt JI, Filiz V, Abetz V. *RSC Advances* 2014; 4: 10252-260.